EES Solar

PAPER

View Article Online
View Journal

Cite this: DOI: 10.1039/d5el00187k

Colour-neutral photovoltaic windows with performance linearly tuneable with transmittance

Shilpi Shital,†[a] Pedro Santos,†[b] Ricardo G. Poeira,[a] Pedro Anacleto,[b] Alice Debot,[a] Chu Van Ben,[a] Michele Melchiorre,[a] Sascha Sadewasser *[b] and Phillip J. Dale *[a]

Received 13th November 2025
Accepted 10th April 2026

DOI: 10.1039/d5el00187k

rsc.li/EESSolar

Building-integrated photovoltaics (BIPV) are predicted to become a cornerstone in the energy transition by enabling on-site electricity generation. While rooftop and opaque façade integrations currently dominate, the widespread use of glass façades in modern architecture presents an untapped opportunity for energy harvesting. This potential remains unexploited due to the absence of suitable semi-transparent photovoltaic (STPV) technologies meeting all requirements, such as suitable average visual transmittance (AVT), spectral quality (expressed as colour rendering index – CRI), and visual comfort (*e.g.* undisturbed views). In this work, we demonstrate the superior optical and electrical performance of a new STPV concept based on interdigitated micro-stripes of chalcogenide solar cells and bare glass. We compare the micro-stripe geometry with ultra-thin absorber approaches both as energy generators and daylight-transmitting windows, evaluating performance across daily and seasonal cycles. Proof-of-concept micro-striped $Cu(In,Ga)Se_2$ STPV devices with AVT ranging from 30 to 70% are demonstrated. Notably, we achieve a record power conversion efficiency of 2.5% at a high AVT of 64% and an excellent 5.8% efficiency at 34% AVT, both with a colour rendering index exceeding 99. These results position micro-striped $Cu(In,Ga)Se_2$ STPV as a highly promising pathway towards power-generating windows.

Broader context

Buildings are estimated to be responsible for 40% of all energy consumption and they are constituted of outer surfaces which are either opaque or transparent. Electrical energy can be generated on opaque surfaces by installing photovoltaic modules. However, modern buildings are trending to have greater transparent surfaces since humans are most comfortable with natural light and unimpeded views. To produce surfaces which both enable daylight transmission and generate electricity is challenging. Previous works based on enduring inorganic materials have ingeniously made photovoltaic devices semi-transparent by sufficiently thinning their absorbing layer or by spatially separating silicon wafers to enable light transmission. In the former case this comes at the cost of having an angularly varying colour and light transmission and thus not providing the integral full daylight spectrum. In the latter case there is an impeded view which is visually disturbing. These two shortfalls can be overcome by using below the eye's resolution micro-solar cells separated by transparent glass. Here, we demonstrate unimpeded neutral coloured semi-transparent photovoltaic devices with high power conversion efficiency potential and highly stable angular dependent optical properties. Using these micro solar cells on transparent surfaces will enable buildings to change from passive energy users to active energy providers.

Introduction

Researchers calculate that between 2 and 9 TWp of photovoltaics needs to be installed in Europe to have a 100% renewable energy system.[1,2] Currently, nearly all photovoltaic installations are either placed inconspicuously on the top of buildings or conspicuously in green fields.[3] Given that buildings are responsible for 40% of the total energy consumed in Europe,[4] interest in building integrated photovoltaics (BIPV) is increasing, where the façades of the building play a dual role of building element and energy-generating surface. Most challenging for BIPV are the light opening apertures or semi-transparent elements in buildings such as atrium, roof or window glasses. Here, semi-transparent photovoltaics (STPV) could play a crucial role, if the stringent requirement of allowing sufficient daylight to pass for human health and activity is fulfilled, whilst also producing a meaningful amount of power. STPV may also find application in agrivoltaics[5] where land is used synergistically for the dual purpose of growing crops and generating power.

STPV are defined by the power conversion efficiency (PCE) and the quality of the transmitted light given by three indices, the average amount of visible light transmitted (AVT) adjusted

---

[a] Department of Physics and Materials Science, University of Luxembourg, 41, Rue Du Brill, L-4422 Belvaux, Luxembourg. E-mail: phillip.dale@uni.lu

[b] INL - International Iberian Nanotechnology Laboratory, Av. Mestre José Veiga S/n, 4715-330 Braga, Portugal. E-mail: sascha.sadewasser@inl.int

† Joint co-authorship.

by the photopic response of the human eye, the colour rendering index (CRI) which describes how well a light source matches the sun's spectrum, and the CIELAB colour coordinates which define its colour.[6] Depending on the precise location and application within the building, low AVT may be acceptable, but human health researchers found that light devoid of blue wavelengths, *i.e.* lower CRI, reduces human cognition.[7] For context, AVT values of 60% and above are regarded as clear, and below 50% are regarded as coloured or reflective.[8] To address these various performance indicators, the performance of STPV is often given as the light utilization efficiency (LUE), which is the product of PCE and AVT ($\text{LUE} = \text{PCE} \times \text{AVT}$), and essentially describes how well the light is used.

There are two main types of STPV, those comprising continuous photovoltaic devices which allow part of the light spectrum to pass through them (Fig. 1a) and those consisting of discontinuous or segmented devices with transparent spaces between them (Fig. 1b). For spatially continuous devices semi-transparency is normally achieved by either using selective UV and NIR absorbing organic molecules[6] or thinning inorganic solar cells' absorber layer such that not all impinging light is absorbed. In the latter case, it is mainly the longer wavelengths of visible light that are not absorbed, leading to predominantly red light being transmitted through the window, and hence a low CRI (Fig. 1d).[9] The segmented approach usually takes the form of silicon wafers spaced apart.[10] For agrivoltaic applications this is unproblematic, but for human window applications the view is strongly occluded, leading to disturbance since the wafers are relatively large and catch the eye's attention as well as leading to a chess board shadowing effect in the interior (Fig. 1e). Note that for the segmented STPV approach, the LUE is defined as $\text{LUE} = \text{PCE}_{\text{TIA}} \times \text{AVT}$, where PCE_{TIA} refers to the PCE of the total illuminated area, which takes the area of the transparent gaps into account. In contrast, in the following we use PCE_{SCA} to denominate the PCE of the solar cell covered area, neglecting the area of the transparent gaps.

Shrinking the size of the solar cells reduces the visual disturbance, as objects below the human eye's acuity limit cannot be resolved. For example, at a distance of ~1 m, the normal human eye cannot resolve features smaller than ~250 μm (Fig. 1f). Nevertheless, it is unnecessary to make their size below human eye's visual acuity limit, since the human eye can change its depth of field to the background and ignore the solar cell foreground occlusion to still obtain meaningful images.[11] To illustrate this approach, Fig. 1g shows a photograph through a laser-printed filter with 260 μm wide black stripes, leading to an undisturbed view of the scenery shown in Fig. 1c. Fig. 1h shows a real-world implementation of such micro-stripes creating a continuous view at Luxembourg airport that allows natural daylight to pass through the window. The stripes are approximately 600 μm wide (Fig. 1i) and the window has an aperture area ratio of 70%. From a viewing distance of a couple of metres the stripes are barely distinguishable, and the eye easily focuses through the window without any disturbance to observe the view outside of the building. Replacing the striped

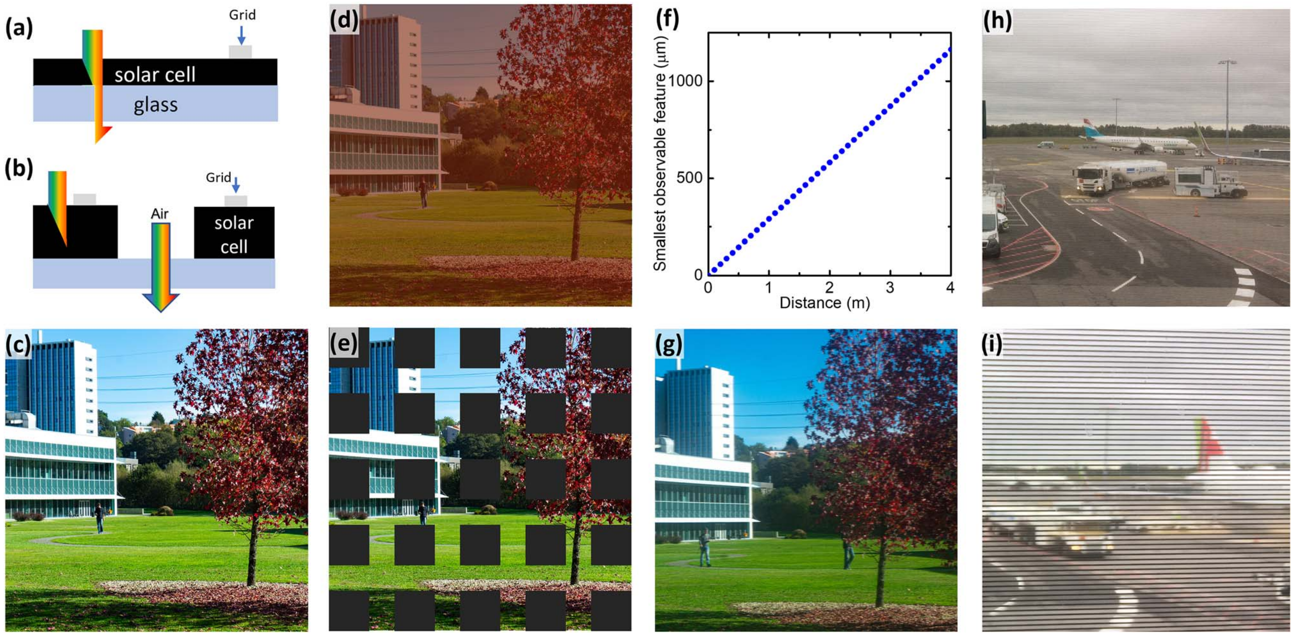

Fig. 1 Representative images depicting two different types of semi-transparent photovoltaic window designs. (a) Schematic side view of a thin absorber PV window that illustrates the blue to yellow light being absorbed in the continuous solar cell, letting the orange to red light pass through. (b) Schematic side view of a segmented PV window. (c) Photograph taken through a regular window, (d) illustration of how a thin-absorber PV window would appear with the orange to red light passing through, and (e) illustration of a segmented PV window based on tiled Si wafers. (f) Human eye's acuity limit, showing the smallest observable feature size as a function of the viewing distance. (g) Photograph of the same scenery as in (c) through a laser-printed filter with narrow black lines (260 μm width, 340 μm spacing) while focusing on the background. (h) Photograph of a real-world implementation of a micro-striped window at Luxembourg airport, with 600 μm wide stripes, permitting nearly unperturbed view, and (i) a photograph taken close-up to the window to reveal the horizontal lines.

filter by solar cell micro-stripes with transparent spaces in-between would lead to a similar semi-transparent appearance.

Recently, semi-transparent devices based on the small solar cell approach have emerged. Lee *et al.* showed proof-of-principle 200 μm thick semi-transparent silicon solar cells perforated with regular arrays of holes of 0.5–100 μm diameter fabricated by energy-intensive deep reactive ion etching.[12] Nevertheless, polycrystalline thin-film solar cell technologies are particularly well suited for this micro-striped STPV concept, since high PCE can be achieved without losses due to edge recombination.[13] Among the thin-film PV technologies, Cu(In,Ga)Se_2 (CIGSe) stands out due to its proven stability, high PCE, absence of toxic elements, and a variety of fabrication processes.[14,15] Indeed, using a high-power laser Sidali *et al.* formed ~500 μm holes in the Mo back electrode and electroplated and annealed Cu(In,Ga)Se_2 (CIGSe) on top to form a 35% transparent mini-module, which suffered from a debilitating series resistance.[16] Very recently, Jeong *et al.* achieved an AVT of 18% and a $PCE_{TIA} = 9.4\%$ mini-module using a high-power laser to ablate a complete Cu(In,Ga)Se_2 device stack with 80 μm wide transparent lines perpendicular to the module's scribing lines.[17] Similarly, laser ablation has been used in perovskite devices to make transparent holes and achieve an AVT of 32% with $PCE_{TIA} = 8.4\%$.[18] Ideally, any STPV fabrication process should have as low energy intensity as possible, as well as be able to easily recover any materials removed. Furthermore, the feature size and the AVT should be flexibly changeable to meet architectural and location requirements.

In the present work, we demonstrate that micro-striped devices allow greater light transmission through the year, and that higher device performance can be expected for comparable nominal AVT's when compared to continuous thin devices with the same absorber band gap. We go on to present a low energy method to fabricate micro-striped solar cells which transmit colour-neutral visible light with extremely high CRI, that are visually non-disturbing, where the AVT is easily scaled, even to high AVT which is scarcely studied. Importantly, the micro-striped solar cells are fabricated using solution-based etching methods, where the component chemical species can be easily recycled. We model and simulate the solar cells to optimise current collection and fabricate devices with different AVT. Finally, our electrical simulations enable us to discuss the challenges that need to be overcome to enable large-area STPV.

Results and discussion

Comparison of thin continuous absorber layer *vs.* micro-striped semi-transparent photovoltaics

A significant body of work in achieving STPV is dedicated to developing solar cells with thin absorber layers that permit a part of the light passing through them to be available for the user behind the window, inside the building. Here, we estimate and compare the AVT and PCE of thin absorber and micro-striped STPVs based on 1.2 eV band gap Cu(In,Ga)Se_2 absorber layers, which is near optimal for single junction solar cells. The power of micro-striped STPV is proportional to the opacity (1 − aperture area ratio) of the cell and shows a linear dependence on the AVT (Fig. 2a), *i.e.* the PCE_{TIA} is simply proportional to the PCE_{SCA} of a perfectly opaque cell multiplied by the fraction of cell area occupied by the absorber layer. The performance of thinned absorber layer STPV follows a more complex relationship with AVT since the absorption coefficient of the absorber layer is not constant above the band gap, and the sun's photon flux also varies with photon energy. Under the generous assumption that open-circuit voltage (V_{oc}) and fill factor (FF) are constant and the PCE_{TIA} of a thin absorber layer device only depends on the number of photons it absorbs, we observe a steep drop-off in PCE_{TIA} from 0 to 5% AVT and thereafter a shallower decline. Note that this assumption neglects any impact of electrical losses, for example, due to increased charge-carrier recombination at the front or back contact interfaces, which become more relevant for thin absorbers in CIGSe solar cells.[19] Comparing the two devices at 45% AVT, the thin absorber solar cell has a thickness of 60 nm with a PCE_{TIA} of 7% whilst that of the micro-striped solar cell is 12%, clearly demonstrating its design advantage.

For laboratory assessment of STPV, the AVT is calculated with a perpendicular light source and detector. However, in real-life applications, the sun is nearly always at an angle, with implications on the performance of STPV as a window. Intuitively, one might expect that for shallow angles of illumination the intensity of the transmitted light differs between the two STPV concepts, thin *vs.* micro-striped. For thin-absorber STPV, light transmission is governed by the Lambert–Beer law for absorption and the increase of the light path in the thin absorber layer as a function of the illumination angle (see left inset in Fig. 2b). In contrast, for micro-striped STPV, the effective AVT for non-perpendicular illumination decreases due to the amount of shadowing that the thin (~3 μm high) micro-striped solar cells cast onto the part of the STPV that is not covered by solar cells (right inset in Fig. 2b). Surprisingly, quantitative assessment of the two cases leads to a rather similar dependence of AVT on the illumination angle (Fig. 2b), which can be attributed to the effect of refraction when the light passes from air through the cover glass into the CIGSe absorber layer. The large refractive index of CIGSe (n ~2.9) leads to a limited increase of the path length in the thin absorber. Nevertheless, due to the wavelength-dependent absorption, the transmitted light colour changes from a light yellow-brown to a much darker brown, as indicated by the colour of the symbols in the figure. Consequently, the CRI for the thin-absorber STPV is lower (~70) compared with that of micro-striped STPV (CRI > 99), which always transmits all colours equally, leading to a neutral grey appearance (see Fig. S1 in SI). The drop of the effective AVT for both STPV concepts at large angles is largely due to an increased reflection off the cover glass (Fig. 2b).

We further assessed the functioning of STPV as a window, considering the light that enters into a building, as the illumination angle (for direct sunlight) changes throughout the day, when the sun moves from east to west and its elevation increases during the morning hours and decreases during the afternoon hours. Fig. 2c illustrates the effective AVT (colour scale) as a function of the time in the day and throughout the year for thin-absorber STPV (left, nominal AVT 33%, thickness

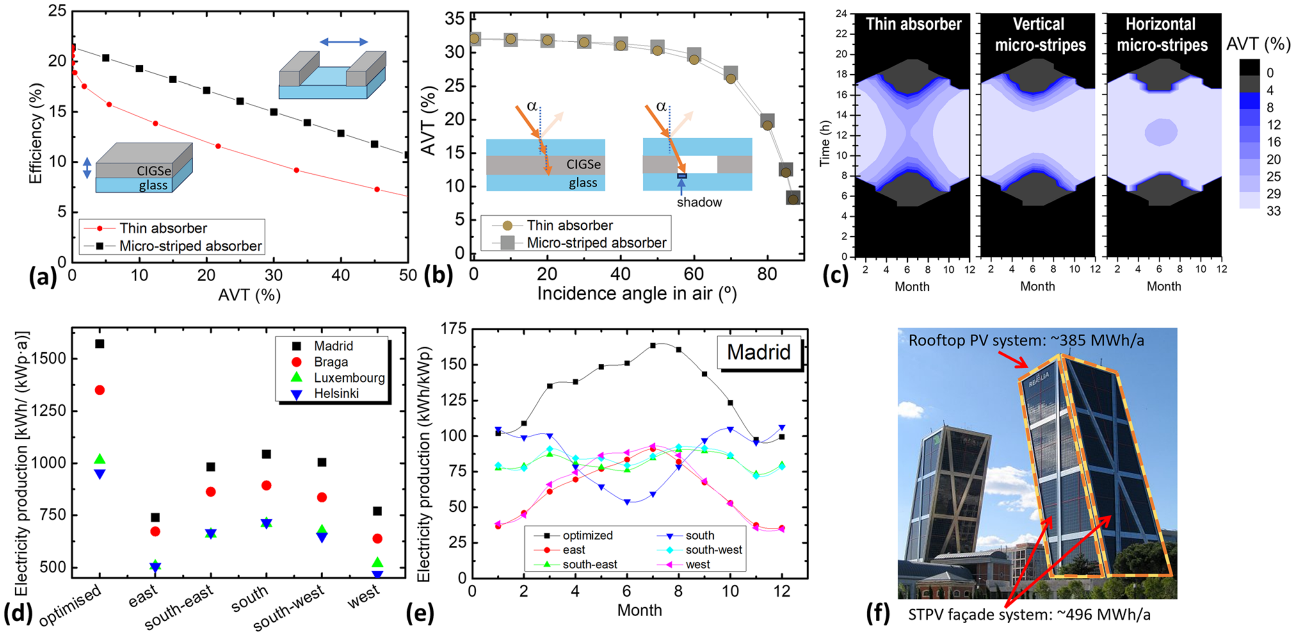

Fig. 2 Comparison of thin-absorber and micro-striped CIGSe STPV devices. Simulated (a) $\mathrm{PCE}_{\mathrm{TIA}}$ as a function of AVT and (b) AVT as a function of the sun's incident angle to the STPV, which has an initial AVT of 32% when the sun is perpendicular to the device. Each data point is coloured by the transmitted light that an observer would see behind the STPV. (c) Effective AVT of thin *vs.* micro-striped STPV (for vertical and horizontal micro-stripes) for a south-facing window in Madrid throughout the day (vertical axis) and year (horizontal axis). The nominal AVT is 33%. Only direct sunlight is considered for simulations in (b) and (c). (d) Predicted annual electricity production for a standard PV system with optimised orientation (*e.g.* rooftop installation) and micro-striped STPV with different window orientations in four European locations (see legend). (e) Monthly electricity production throughout the year for Madrid. Note that systems mounted on south-east or south-west façades will produce nearly a constant level of electricity throughout the year, with little seasonal variation. (f) Illustration of the annual electricity production for a rooftop PV system compared with 50% semi-transparent PV systems mounted on the south and east façades of the "Gate of Europe" building in Madrid. Simulations in (d), (e) and (f) consider the appropriate composition of direct and diffuse sunlight according to the PVGIS database. Photograph by Osvaldo Gago, retrieved from https://commons.wikimedia.org/wiki/User:OsvaldoGago/Madrid#/media/File:PlazaCastillaMadrid.JPG. The original photo was modified to include the dashed lines indicating the STPV-covered façades.

= 92 nm), and micro-striped STPV (nominal AVT 33%, stripe width = 200 μm, distance between stripes = 100 μm, stripe height = 3 μm) for a south-facing STPV in Madrid. For micro-striped STPV, we further differentiate vertical (middle panel) and horizontal stripe geometry (right panel). Despite the similar angle dependence (Fig. 2b), in an actual application, the two STPV technologies behave differently. The effective AVT for thin-absorber STPV exhibits a stronger variation, as in this case the combination of azimuth angle and elevation is relevant, while for micro-striped STPV only the azimuth angle (for vertical micro-stripes) or the elevation (for horizontal micro-stripes) is relevant. The effective AVT for the thin-absorber STPV remains above 20% for most of the day and year. Nevertheless, the impact of the micro-striped STPV on the transmitted light is much weaker, with the least impact as function of time and day for the horizontal stripe configuration, which exhibits AVT above 25% most of the time. Note that only direct sunlight is considered here; diffuse light will be transmitted for both STPV approaches similarly, following the angular dependence shown in Fig. 2b.

To analyse the performance and energy yield of micro-striped STPV, we compare vertically mounted micro-striped STPV windows on different façades in different locations (Madrid, Braga, Luxembourg, Helsinki). Fig. 2d shows the annual electricity production per installed kWp of STPV mounted as vertical windows with east to west orientations. As expected, south-facing windows exhibit the highest energy yield, which drops off when the windows' orientation changes toward east or west. The south-facing STPV window system generates about 65–75% of the power of a standard PV system mounted with an optimised orientation (for example a rooftop installation). Note that the total STPV window area per installed kWp is 1/(1-AVT) times larger than that of a standard opaque PV system. Thus, for a system with 33% AVT, the required window area is 50% larger than that of a standard PV system with same nominal output power. Obviously, the energy yield of the micro-striped STPV system depends on the general climatic conditions and the latitude of the location. Curiously, relative annual electricity production of STPV compared to that of an optimally-oriented PV system improves the further north (south in the southern hemisphere) the system is installed (see Fig. S2 in SI), which is due to the lower sun elevation and consequently smaller deviation of the vertical STPV mounting from the optimised installation inclination. Another relevant performance indicator is the seasonal variation of the electricity production. While the standard PV system with optimised orientation shows the expected peak in electricity production in the summer months (Fig. 2e for Madrid and S3 in SI for the other selected locations), a south-facing STPV system actually shows a decrease in the electricity production in the summer. This reduction is due to the vertically-mounted STPV window and the high elevation of the sun in the summer months. Interestingly, façades facing south-east or south-west exhibit very little (less than 25%) seasonal variation, producing only 6% less electricity over the year compared with the south-facing façade. This consistent power production throughout the year is beneficial for electrical grid operators in mitigating seasonal variations. At the same time, the typical duck curve for the daily variation of electricity production could also be mitigated by avoiding south-facing façade installation.[20] Finally, we illustrate the potential of the micro-striped STPV on a real-life building, the "Gate of Europe" towers in Madrid (Fig. 2f). Using STPV windows for all glass elements in the south and east facing façades of one tower would enable to generate an additional ∼0.5 GWh per year to a rooftop system, which would be limited to less than 0.4 GWh per year, thus more than doubling the PV capacity of this building.

Modelling and simulation of micro-striped solar cells

Since we have clearly established the benefits of micro-striped STPV modules, the next step is to investigate the front contact current collection for individual solar cell stripes connected in parallel. The design of the device is shown in Fig. 3a. The $\mathrm{PCE_{SCA}}$ of a single cell stripe will depend on the short-circuit current density (J_{sc}) and the fill factor (FF), while the open-circuit voltage (V_{oc}) stays constant. For a fixed AVT, the J_{sc} depends on the transparency of the conducting ZnO : Al window layer and the shadowing caused by the metal grid finger over the absorber layer. The FF mainly depends on the sheet resistance of the window layer and the dimensions of the grid finger. Therefore, improvements to the J_{sc} will worsen the FF: a thinner window layer will improve its transparency and thus raise J_{sc}, but the higher sheet resistance will lead to a lower FF. Likewise, a narrow grid finger reduces shading and increases J_{sc}, but also increases its resistance, again decreasing the FF. Since the sheet resistance of the metal grid line used for CIGSe solar cells is typically three orders of magnitude lower than the commonly used window layers (0.02 Ω cm *vs.* 10–70 Ω cm),[21] current along the length of the stripe will mainly flow through the grid finger rather than in the window layer.

We modelled a single micro-stripe of the solar cell by breaking it into discrete elements and representing each element as a one-diode solar cell model where the current can flow to the next element either through the window layer or through the metal grid. Details of this approach are given in the supplementary information. Given that the window layer resistivity cannot be lowered significantly without reducing its transparency, we focused on optimising the grid finger dimensions to find the optimum balance between J_{sc} and FF.

Fig. 3 schematically depicts a part of the solar cell device, which is constrained to stripe lengths of 2.4 cm, a width of 400 μm to match our fabrication capabilities and an AVT of 30%; larger length scales are considered in the "Scaling up" section below to understand the effect of scale-up necessary for actual deployment. The current generation in the absorber layer is uniform everywhere so the current flowing through the metal grid finger increases linearly from the back contact towards the front contact. Burgers has shown that a tapered grid finger, narrower near the back contact (w_{BC}) and wider at the front contact (w_{FC}), is well suited to collect current along a stripe.[22] Fig. 3b and c show that with increasing width of the grid finger on either side, the FF increases and the J_{sc} decreases. The open-circuit voltage (not shown) stays almost constant. The highest total illuminated area $\mathrm{PCE_{TIA}}$ as a result of these trade-offs is 11.4% for 30% AVT and can be achieved with a grid finger width of w_{FC} = 15–20 μm at the front contact side and w_{BC} = 1 μm nearest the back contact (Fig. 3d). This compares well to the ideal $\mathrm{PCE_{TIA}}$ of ∼12% for the same solar cell stripe with zero resistivity TCO and no grid, which corresponds to the expected performance for 30% AVT considering $\mathrm{PCE_{TIA}}$ = 17.1% for the opaque solar cell as starting point (see Table S1 in SI). The optimised grid parameters for the other stripe width (1000 μm) considered to be experimentally fabricated are shown in Fig. S6 in the SI. Essentially, as the cell stripe width increases, the grid finger w_{FC} also has to increase to achieve a similar efficiency.

Experimental fabrication of micro-striped solar cells

The fabrication process involves selectively removing material from large-area thin film solar cell stacks to reveal stripes by

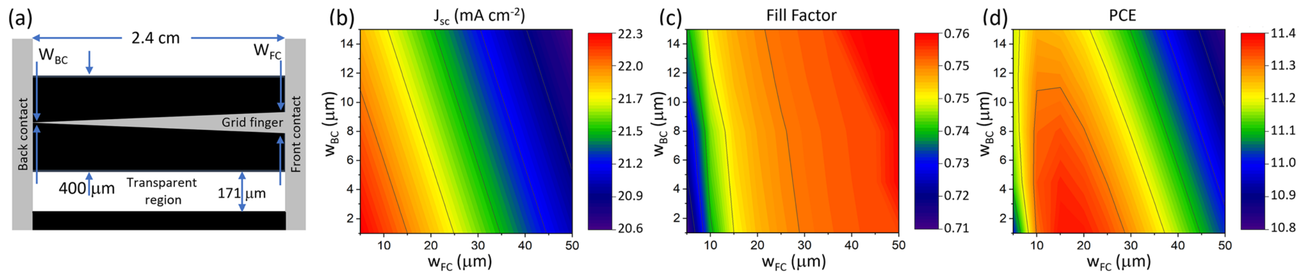

Fig. 3 Optimisation of grid finger geometry for micro-striped STPV by simulation. (a) Design (not to scale) of the grid finger (grey) on the micro-line solar cell stack (black, Mo/Cu(In,Ga)$\mathrm{Se_2}$/CdS/i-ZnO/ZnO : Al) with width = 400 μm and length = 2.4 cm and an AVT of 30%, considering a tapered grid finger of 2 μm thick Ni/Al metal, with w_{BC} and w_{FC} as the width nearest the back contact and at the front contact, respectively. Simulated (b) J_{sc}, (c) FF, (d) total illuminated area $\mathrm{PCE_{TIA}}$ as a function of grid width parameters using the reference cell data of Table S1 in SI. The V_{oc} of all stripes is similar with an average value of (691 ± 3) mV.

using a combined photolithography and wet etching approach (see Fig. 7 in the Methods section). In preliminary work, we established the veracity and capabilities of this approach by fabricating individual solar cell stripes with widths of 200 to 1000 μm and a length of 0.8 cm (see Fig. S7 in SI).[23] We found that we could make devices with stripe widths above 400 μm with a solar cell covered area $\mathrm{PCE_{SCA}}$ close to that of the large area standard-sized cells whilst for the 200 μm stripes the $\mathrm{PCE_{SCA}}$ was significantly reduced (Fig. S7 in SI). Initial electron microscopy investigations revealed that the etching process removed the ZnO-based window layers laterally faster than the CIGSe absorber layer, resulting in a reduction of the current collection area and, consequently, a decrease in J_{sc}.

As a first step to go to larger sizes, we chose to increase the stripe length from 0.8 to 2.4 cm and fabricated solar cell stripes with widths of 400 and 1000 μm separated by 400 and 1000 μm, respectively, corresponding to a nominal aperture area ratio (AA) percentage (100 × (total area − solar cell striped area)/total area)) of 50% (Fig. 4a). These samples are denoted 50AA400S and 50AA1000S, respectively. As suggested by our simulations in the previous section, tapered front contact grid lines were used with $w_{\mathrm{FC}} = 20$ μm (40 μm for the 1000 μm wide stripes) and $w_{\mathrm{BC}} = 2$ μm, which maximises the efficiency by balancing the impact on J_{sc} and FF. After fabrication, the lateral etching of all the layers in the device structure was assessed using confocal microscopy (see Fig. S8 in SI). The planned 1000 μm stripes had their solar cell stripe areas reduced slightly, leading to a measured aperture area ratio of 52%. For the 400 μm stripes, the lateral etching was slightly larger and the measured aperture area ratio was 56%.

Current–voltage (JV) characteristics of individual solar cell stripes are shown in Fig. 4b, and the measured average solar cell parameters of the individual stripes are given in Table 1. For both stripe widths, a high V_{oc} is observed, close to the reference device. Regrettably, the J_{sc} is lower for all the devices compared to the reference device. Most of the J_{sc} loss is due to the lateral etching of the layers which make up the device stack, affecting the window layer more than the rest of the layers (Fig. S8 in SI), therefore reducing the current collection area of the stripes to ∼82% of the striped area (see Fig. S9 and Table S2 in SI). Note that in the following we use the solar cell covered area $\mathrm{PCE_{SCA}}$, which is normalised to the opaque area of the device (excluding the transparent gaps); this area is larger than the active collection area of the stripes (see Table S2 in SI for more details about the various relevant areas). Overall, the individual stripe $\mathrm{PCE_{SCA}}$ lie between 9 and 13%, which is somewhat lower than the reference cell PCE of 17%. By averaging the stripe area PCEs, the

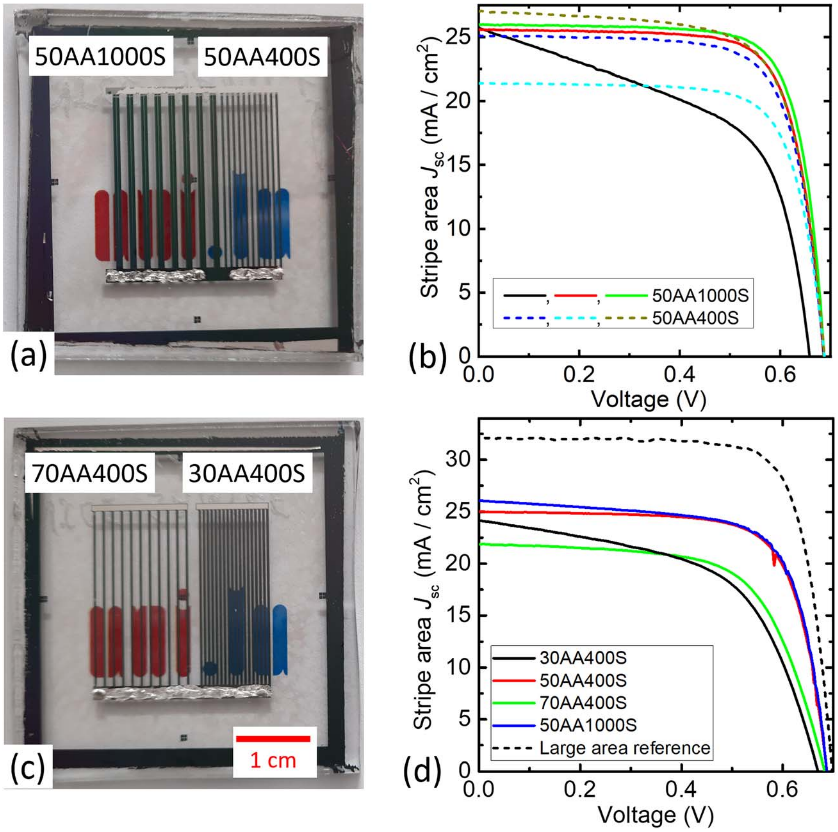

Fig. 4 (a) Photograph of STPV devices with 1000 μm (left) and 400 μm stripes (right) with 50% nominal aperture area ratio and (b) selected current–voltage curves of individual stripes (c) photograph of STPV devices with 400 μm stripes with 70% (left) and 30% (right) nominal aperture area ratio and (d) current–voltage curves of the full devices comprising 11 and 18 stripes for the 70% and 30% nominal aperture area ratio STPV devices, respectively, normalised to the total solar cell striped area. For comparison, JV curves of the reference cell as well as the average of the 50% nominal aperture area ratio STPV devices are also shown.

Table 1 Nominal and measured aperture area, measured average visual transmittance (AVT), and photovoltaic performance parameters of the fabricated STPV devices, considering the total area of the devices and just the solar cell stripe areas. (*) For the STPV devices with 50% nominal aperture area, the electrical performance values given are the average of the individual stripe measurements

	Full STPV device				Solar cell stripe areas only			
	Nominal aperture area ratio (%)	Measured aperture area ratio (%)	AVT (%)	PCE_{TIA} (%)	PCE_{SCA} (%)	J_{sc} (mA cm^{-2})	V_{oc} (mV)	FF (%)
50AA400S	50	56	49	5.5*	12.5*	25.0*	687*	72.9*
50AA1000S	50	52	49	6.1*	12.7*	26.2*	682*	71.5*
30AA400S	30	36	34	5.8	9.0	24.2	669	55.7
70AA400S	70	74	64	2.5	9.6	21.9	683	64.1

total illuminated area PCE_{TIA} is also estimated in Table 1, using the measured aperture areas of 52% and 56%, respectively.

Subsequently, we also fabricated micro-striped STPV devices with electrically connected stripes, forming thus a single device. Two different transparencies were realised, with 70% and 30% nominal aperture area ratio and 400 μm wide solar cell stripes in both cases (Fig. 4c, devices 70AA400S and 30AA400S, respectively). The lateral etching was again assessed using confocal microscopy (see Table S2), disclosing measured aperture area ratios of 74% and 36%, respectively. The *JV* characteristics of the full devices (comprising 11 and 18 stripes, respectively) are shown in Fig. 4d, and the device parameters are given in Table 1. Note that the current density in the figure considers only the solar cell stripes and not the full device area. The device 30AA400S shows a drop in fill factor relative to 70AA400S, likely related to the peeling of some parts of the metal grid lines during the fabrication process (see Fig. S10 in SI). Again, the J_{sc} is lower for these two STPV devices compared to the reference device for the same reasons discussed above. The solar cell covered area PCE_{SCA} lie around 9% which is somewhat lower than the individual stripes of the devices with 50% nominal aperture area ratio discussed above. Besides the PCE_{SCA} of these devices, also the total illuminated area PCE_{TIA} was calculated using the measured aperture area ratio (see Table 1). Logically, 70AA400S is the least performant since nominally only 26% of the area is used for power conversion. For the device 30AA400S, a PCE_{TIA} of 5.8% was achieved. To see how these micro-striped solar cells compare against other semi-transparent devices, their optical properties need to be assessed.

The visual aspect of the micro-striped solar cells was investigated by examining and looking through them, as well as measuring their respective transmission spectra. Fig. 5a–d show photographs of the devices, where one picture was taken from a 30 cm distance with focus on the device, and another picture was taken from the same distance with focus on the building behind. This demonstrates the two views that an observer will have, depending on what they are focussing on. When focussing on the STPV devices all stripes are visible for a 30 cm viewing distance, whilst at about 1.4 m the human eye cannot distinguish the 400 μm stripes (see Fig. 1f). When focussing on the background, the individual 400 μm stripes are no longer discernible for any aperture area, whilst the 1000 μm stripes are discernible near the edges of the bus bars. These also become indistinguishable if the distance between the viewer and the micro-striped solar cells becomes larger (about 3.5 m). The different aperture areas are clearly distinguishable in Fig. 5b and d with the opacity scaling accordingly, and no coloured tint can be observed, showing the smooth transmission of white light. To confirm that the light is transmitted at all wavelengths equally in the visible range, transmission spectra of the devices were measured (Fig. 5e). All device types show a virtually flat response across all wavelengths. From the transmission spectra data, the AVT is calculated considering the human eye's photopic response,[6] finding AVT = 34, 49, 49, and 64% for the STPV device types 30AA400S, 50AA400S, 50AA1000S, and 70AA400S, respectively (a discussion of the uncertainty of these AVT values is provided in the SI). It should be noted that the AVT is in all cases lower than the aperture area ratio due to the reflection from the glass between the solar cell stripes. The transmission of the 50AA400S and the 50AA1000S are similar despite having slightly different effective aperture area ratios.

To compare our micro-striped approach to the thin absorber approach, Fig. 5f shows an overview of the PCE_{TIA} as a function of AVT for many CIGSe literature devices. As predicted by our calculations (see Fig. 2a), the continuous thin absorber CIGSe devices' PCE_{TIA} decreases with increasing AVT as the absorber layer thickness is reduced (circles). Even a 30 nm thick absorber layer only achieves an AVT of 56% with a PCE of 1.7%,[24] demonstrating how challenging it is for thin absorber approaches to reach high AVT values. In contrast the micro-striped approach enables high AVT whilst keeping higher PCE_{TIA}. This is illustrated in Fig. 5f by a simplistic estimate of maximum PCE_{TIA} *vs.* AVT (solid line), which neglects optical losses from the glass and grid reflections and assumes perfect current collection. Our STPV devices' measured performance follows the trend of the line with the 50AA1000 s device lying closest to the line, reflecting the least current losses. The only other micro-striped CIGSe device is a mini-module reported by Jeong *et al.*, which has a lower AVT (18%, square symbol) than our micro-striped solar cells, making a direct comparison of the PCE_{TIA} difficult.

A further feature of the micro-striped approach is its colour neutrality. The colour of the data points in Fig. 5f, g, and h corresponds to the colour of light that would be transmitted through the devices if illuminated by the sun. For the thin absorber devices, the colour starts as dark brown at low AVT and changes to lighter yellow at high AVT. In contrast, the micro-

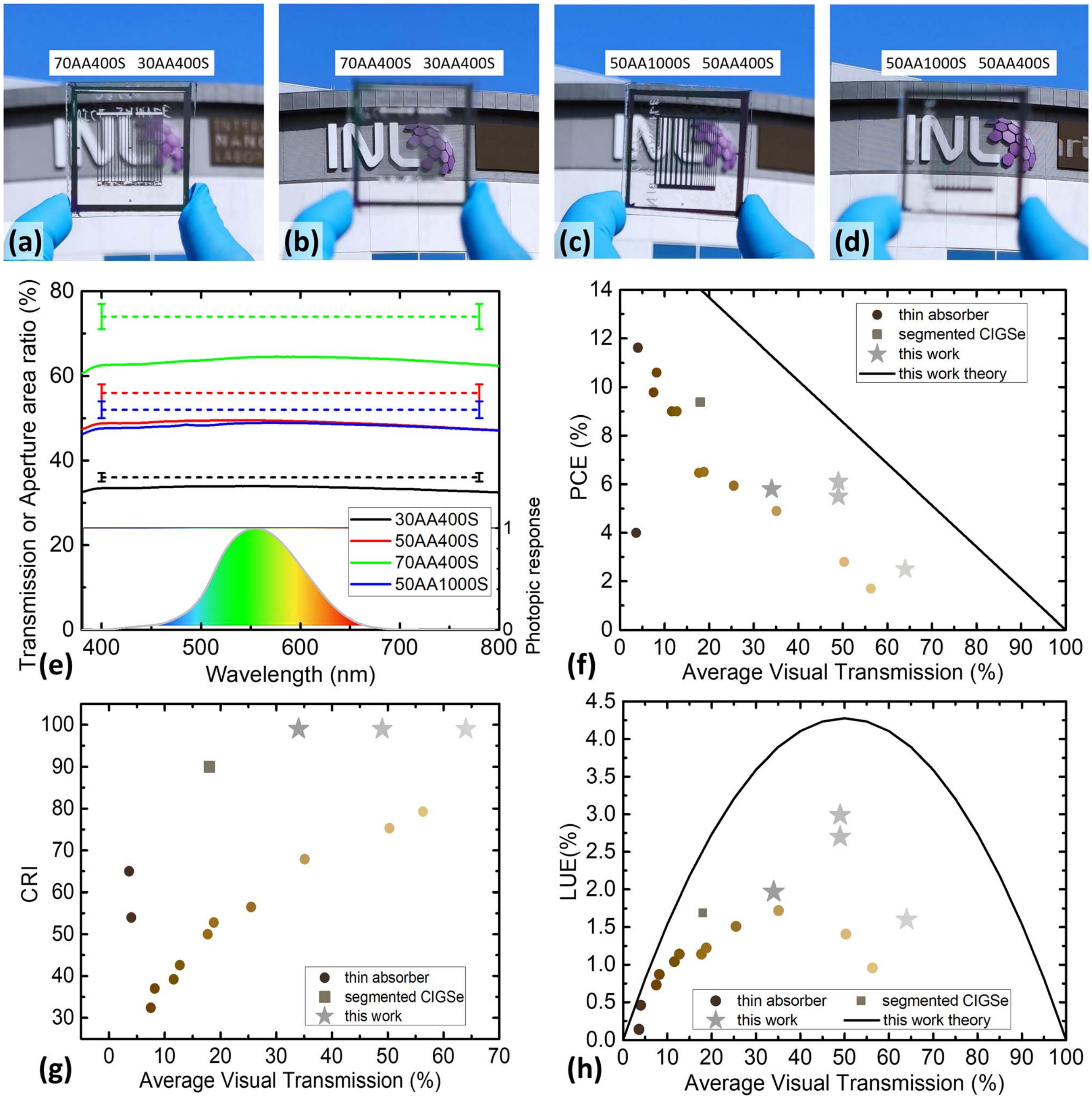

Fig. 5 Visual appearance of the fabricated STPV devices with 70% and 30% nominal aperture area ratio with solar cell stripe width 400 μm with (a) focus on the micro-stripes and (b) focus on the background, and 50% nominal aperture area ratio with solar cell stripe widths of 1000 μm and 400 μm with (c) focus on the micro-stripes and (d) focus on the background. (e) Transmission of the micro-striped STPV devices (average of three measurements – solid lines) and measured aperture area ratio (dotted lines). The bottom part shows the photopic response of the human eye, relevant for determining the AVT according to ref. 5. (f) PCE_{TIA}, (g) CRI, and (h) LUE as a function of AVT for our STPV devices as well as selected literature works (see Table S3 SI).

stripes of this work appear grey as they transmit all colours equally. For further confirmation, we plot the CRI in Fig. 5g, and although the thin absorber devices have improved CRI with higher AVT, they never exceed 80, unlike our STPV devices, which all have a CRI above 99. Another way to compare technologies is by the light utilization efficiency (LUE). The LUE has a parabolic shape with a maximum at 50% AVT (Fig. 5h). Our STPV devices, as well as that of Jeong *et al.*[17] have higher values than the continuous thin absorber approach for a given AVT, with peak LUE values at 50% AVT. Note that Jeong *et al.*[17] reported a series-interconnected mini-module, for which dead area in the interconnect reduces PCE_{TIA}, which needs to be considered when comparing PCE and LUE values. Interestingly, for the thin absorber approach, peak LUE values are found around 35% AVT. This shift in peak LUE value to lower AVT might be assigned to difficulties in maintaining high fill factor and open-circuit voltage for the ultra-thin CIGSe absorber layers. On the other hand, the increased edge surface created by the micro-stripes does not appear to be too harmful, as the voltage and fill factors remain high. Indeed, Paire *et al.*[13] reported that CIGSe micro solar cells fabricated by a similar chemical etching process have passivated edges and do not suffer from edge recombination.

Fully colour neutral approaches, with CRI ≥ 95 have recently been investigated by either making openings in silicon and perovskite solar cells[12,18,25] or using UV and NIR absorbing molecules.[8] Our STPV devices' LUE values are slightly lower than those of the silicon and perovskite technologies (see Fig. S12 in the SI), which we attribute to the higher initial efficiencies of the full-area devices compared with those of our micro-striped solar cells before the etching process. In summary, we have demonstrated here that for the CIGSe material system, using full thickness solar cells with micron-sized openings to transmit light leads to higher $\mathrm{PCE_{TIA}}$, access to higher AVT, and a colour neutral view.

Scaling up to large areas

Following the successful demonstration of a proof of concept for achieving high AVT colour neutral micro-striped STPV devices with high CRI, it is now required to consider longer stripe lengths to address the future commercial application of micro-striped STPV. Simply extending the length of the cell stripes will increase the series resistance of the grid, thus decreasing the solar cell performance. As an example, we compute the cell parameters as a function of grid width for a 30% AVT STPV device with 25 cm solar cell stripe length (Fig. S13 in SI), ten times longer than the grid optimisation (Fig. 3) for our experimental proof-of-concept devices. The relative trade-off between J_{sc} and FF follows the same trend as for the shorter stripes, but here, the $\mathrm{PCE_{TIA}}$ is limited to 6.7% due to the larger resistance stemming from the longer grid lines required for the longer solar cell stripes. One possibility to reduce the series resistance of the grid finger is to make it thicker. The previous calculations were done for a 2 μm thick Ni/Al grid, which is normally used on CIGSe solar cells. In Fig. 6, we compare the solar cell parameters for grid fingers with 2, 6, and 9 μm thickness applied to solar cell stripes up to 50 cm long and 400 μm wide (optimised grid widths are given in Fig. S14 in SI). The increase in grid height improves the FF without reducing the J_{sc}, with the effect being most significant for the longest stripes. For 50 cm stripe lengths the $\mathrm{PCE_{TIA}}$ is dramatically improved from below 4% up to 7% and for 10 cm long solar cell stripes, the 9 μm thick grid lines help retaining ~90% of the ideal efficiency. Further increases in the grid height would improve all parameters for the longest stripe lengths but eventually there would be a trade-off against increased shadowing losses due to the grid lines casting a shadow when the sun illuminates at a flat angle. These simulations and discussions indicate that colour-neutral STPV are capable of delivering practical efficiencies at commercially relevant scales. Further upscaling to full-size modules is possible by using monolithic series interconnect along the micro-stripes.

We note here that for industrial viability, also the economic aspects need to be considered, which is out of the scope of the present work. Nevertheless, relevant points to consider are the cost of the photolithography processes used in the present work for the definition of the micro-stripes and grid lines. Alternatives to the photolithography processes are the use of laser-scribing for the micro-stripe formation and the use of screen-printed grid lines, processes well established already for the series interconnection in thin-film modules and the top contacts in Si PV, respectively.

Materials and methods

Simulation methods

Performance comparison between continuous thin absorber and segmented semi-transparent photovoltaics. Solar cell parameters of a previous world record CIGSe device[26] (see Table S5 in SI) were used as a basis to calculate the different power conversion efficiencies (PCE) as a function of AVT of the continuous and segmented micro-striped STPV devices under AM1.5 G illumination. For the continuous thin absorber device, we replaced the molybdenum back contact with transparent indium-doped tin oxide. The light absorbed in the CIGSe absorber and the light transmitted through the back electrode were calculated using the transfer matrix method. Using the transmitted light, the AVT was calculated for different CIGSe thicknesses following ref. 6 and J_{sc} was calculated from the

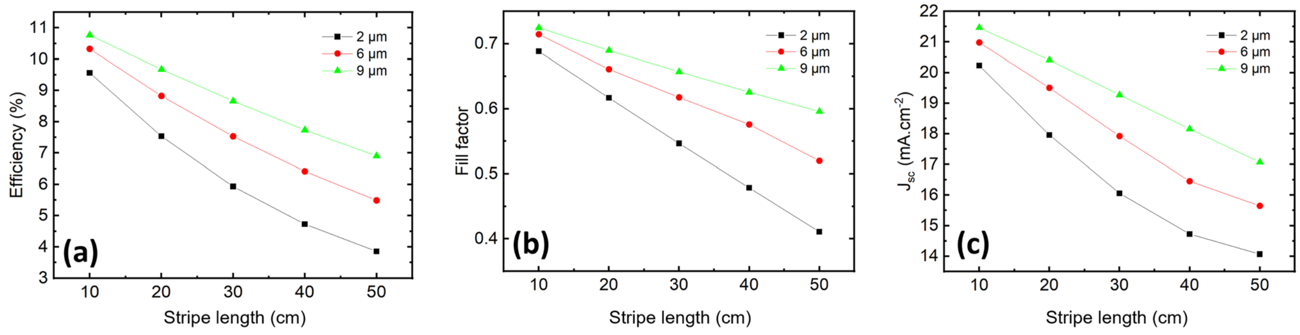

Fig. 6 Total area JV properties for STPV devices with 400 μm wide stripes and 30% AVT. (a) $\mathrm{PCE_{TIA}}$, (b) fill factor, and (c) J_{sc}. A near constant V_{oc} of 697 mV is found for all stripe lengths.

Table 2 Experimental reference cell parameters taken from the median 0.5 cm^2 area device of eight devices

PCE_{TIA} (%)	J_{sc} (mA cm^{-2})	V_{oc} (mV)	FF	J_0 (A cm^{-2})	R_s (Ω cm^2)	R_{sh} (Ω cm^2)	n
17.1	32.1	697	0.76	1.5×10^{-9}	0.44	1943	1.57

absorbed light in the CIGSe layer assuming a 90% collection efficiency. The PCE was then calculated from the J_{sc} assuming that the open-circuit voltage and fill factor remain invariant. See supplementary information for full details.

To determine the angular dependence of the AVT we calculated the intensity of light transmitted through the device. For this assessment, a cover glass (refractive index $n_{glass} = 1.5$) was included, considering reflection and refraction into the glass and the CIGSe absorber. Other layers of the CIGSe solar cell device were neglected for simplicity. For the thin absorber, 92 nm thickness was selected to achieve an AVT of 33%. Light absorption in the CIGSe absorber layer was calculated for different incident angles using the Lambert–Beer law, considering refraction into the glass and the CIGSe absorber ($n_{CIGSe} = 2.9$), with subsequent calculation of the AVT from the resulting spectra.

For the segmented micro-striped device, the PCE_{TIA} was calculated by multiplying the reference device PCE by (1-AVT) with the desired AVT. The angular dependence of the AVT was calculated by considering the area of shadow created by a stripe of 3 μm thickness and 200 μm width as a function of the position of the sun. Reflection from and refraction in the cover glass were considered to ensure comparability with the assessment for the thin absorber STPV.

For the assessment of the electricity production of the STPV, the Joint Research Center's (JRC) Photovoltaic Geographical Information System (PVGIS) was used, with details given in the supplementary information.[27]

Simulation and optimisation of current collection of segmented solar cells. To simulate the optimum grid finger profile for different solar cell stripe widths, we used a lumped diode model.[28] Due to symmetry, only one half of a single cell stripe needs to be considered and is assumed to be made of tiny elements (Fig. S4 in SI). Laterally, the current can flow through the window layer made of ZnO:Al or the metal grid finger made of Ni/Al. Hence, each tiny element was modelled using a one-diode solar cell model with the window and grid finger's resistances represented separately so that they could be varied to find the optimal current collection. Three lumped resistances were used for the window layer to reflect the different directions that the current could flow,[29] and were calculated from the sheet resistances of the respective layers. The one-diode parameters were estimated from a one-diode fit of the measured JV curve of the reference solar cell. The extracted solar cell parameters are given in Table 2 (for details see SI).

The device simulations were done using LTSpice.[30] The input file was written using Python with the help of the library

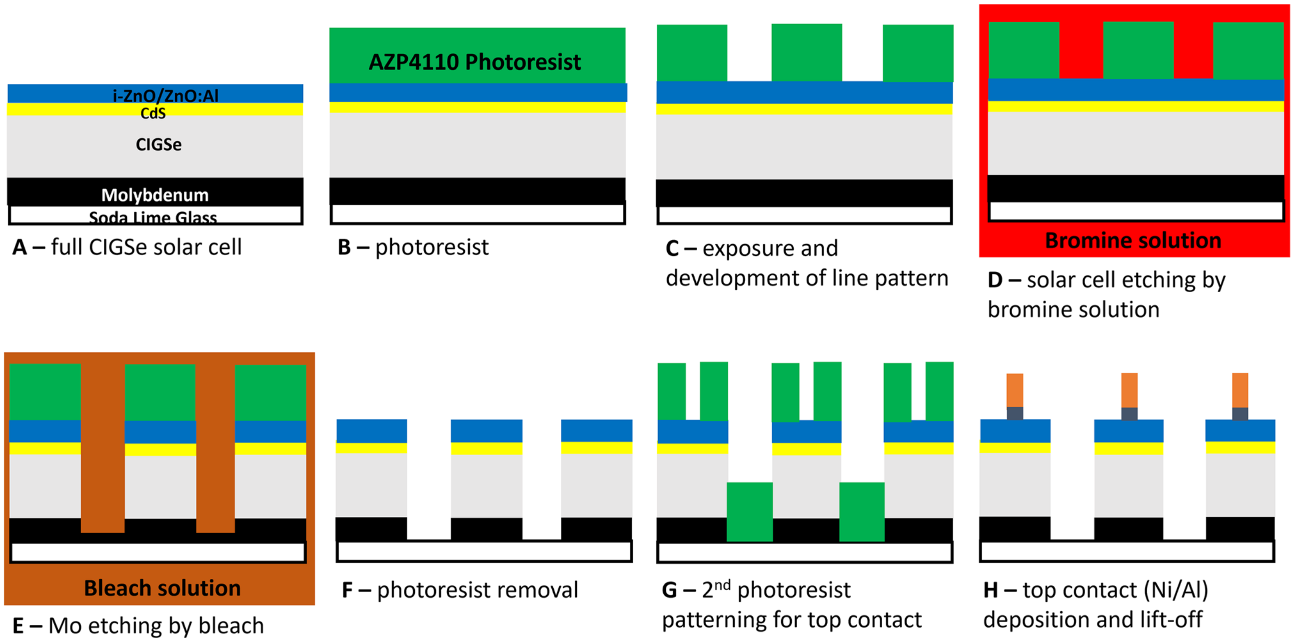

Fig. 7 Fabrication process for the micro-structured semi-transparent $Cu(In,Ga)Se_2$ solar cells, starting with (A) a full CIGSe solar cell stack on a SLG substrate with Mo back contact, CIGSe absorber layer, CdS buffer layer and i-ZnO/ZnO:Al window layer. (B) Photoresist is spin-coated onto the CIGSe solar cell, and (C) the desired line pattern is exposed with a direct write laser and subsequently the resist is developed. (D) Aqueous bromine solution is used to etch the CIGSe solar cell stack in the desired locations not protected by photoresist, after which (E) the remaining Mo layer is etched by bleach. After (F) photoresist removal with acetone, (G) a second photolithography process is applied to deposit (H) Ni/Al front contact lines onto the CIGSe micro-lines.

'PyLTSpice'.[31] Our optimisation tries to balance between improvements in J_{sc} and losses in FF as a result of changing the width of the grid for the best device efficiency (η). Multiple local efficiency maxima are possible, so we used a genetic algorithm implemented by Python library 'Pygad' to find the global maximum.[32] Once the optimum current–voltage properties of the half stripe were calculated, the electrical and AVT properties of the whole STPV device were calculated from considerations of symmetry.

Experimental methods

Solar cell devices were prepared on 50 × 50 mm^2 soda-lima glass (SLG) substrates with a structure of SLG/Mo/CIGSe/CdS/i-ZnO/ZnO:Al. The SLG/Mo/CIGSe was industrially sourced (NICE Solar), whilst the 50 nm CdS was deposited by chemical bath, and the 80 nm i-ZnO and 380 nm ZnO:Al were sputtered (Orion-8, AJA). The micro-structuring fabrication (Fig. 7) starts with a lithography step, where a layer of photoresist (AZP 4110 positive resist, MicroChem, Ulm, Germany) is coated onto the device stack and the desired solar cell stripes design is patterned (Fig. 7C). Subsequently, the device stack is submitted to 0.1 M aqueous bromine solution for 13 min (Fig. 7D), followed by sodium hypochlorite (commercial bleach, <5% NaOCl) solution (Fig. 7E) for 1–2 min in an ultrasound bath at room temperature to completely remove the molybdenum. The final steps in the mini-window fabrication process consist of a second lithography step (Fig. 7G) and a subsequent evaporation of a 2 μm Ni/Al metal contact (Univex-300) and lift-off process (Fig. 7H), to ensure that a proper charge collection along the solar cell stripe is achieved. The lithography patterning steps were performed with a direct write laser (DWL 2000, Heidelberg Instruments).

The etched devices were analysed by scanning electron microscopy (SEM) in a FEI Quanta 650 FEG SEM microscope. To evaluate the impact of the etching process on the edges of the stripes, confocal microscope analysis was performed using a Keyence VK-X1000 system, equipped with a 404 nm laser, using 5X, 20X and 150X objectives. The *JV* characteristics of the fabricated devices were characterised in an Oriel Sol3A class AAA solar simulator under AM 1.5 illumination at room temperature.

Transmittance measurements were performed using a PerkinElmer Lambda 950 UV–Vis–NIR spectrophotometer equipped with an integrating sphere. Calibration was carried out by recording the transmittance under illuminated and dark conditions using a Spectralon reference standard, thereby defining the 100% and 0% transmittance baselines. A monochromatic beam was directed onto the sample, which was positioned at the centre of the integrating sphere. The wavelength was scanned from 300 to 900 nm. The incident beam had a rectangular cross-section measuring 5 mm in height and 3 mm in width. For each sample, three measurements were taken at different locations.

Conclusion and outlook

Using geographical solar radiation data, we showed that segmented semi-transparent photovoltaics (STPV) vertically mounted as electricity-generating windows can contribute significantly to the generation of on-site electricity in cities. The annual energy yield of a south-facing façade was shown to be as high as 65–75% of that of an optimally oriented rooftop system, depending on the latitude. We assessed the optical performance of the commonly considered semi-transparent thin absorber technology compared with the novel micro-striped STPV technology. In a real-life STPV window application, the angle of incidence varies throughout the day and year and hardly ever matches the lab-based performance assessment under perpendicular illumination. Thin-absorber STPV suffers from a stronger variation in transmittance throughout the day and seasons, while micro-striped STPV can maintain close to nominal transmittance throughout most of the day and the year. Furthermore, micro-striped STPV exhibits significantly higher CRI values, clearly demonstrating the design superiority of this novel STPV technology.

We fabricated proof-of-concept STPV devices by selectively etching transparent micro-stripes into full area Cu(In,Ga)Se$_2$ (CIGSe) solar cells, leading to STPV devices with 34 to 64% AVT and power conversion efficiencies (PCE$_{TIA}$) between 6.1 and 2.5%, among the best-performing CIGSe STPV devices. Importantly, these devices present a non-disturbing view with white light transmittance corresponding to a colour rendering index above 99. Advantageously, the micro-striped architecture's key performance indicators, namely PCE$_{TIA}$ and AVT, scale linearly with the active photovoltaic area, making the technology easy to adapt to different geographical locations and desired uses. Finally, using electrical simulations, we show a way forward to upscaling micro-striped solar cells to larger area windows, a first important step toward exploitation of the beneficial performance characteristics of this STPV technology. Furthermore, the micro-striped concept for STPV can be applied to other thin-film solar cell technologies, such as perovskites, organic PV and emerging inorganic PV based on earth-abundant elements.

Author contributions

PD and SaS developed the concept for the study and supervised the work. ShS, SaS, and PD wrote the manuscript. ShS calculated the efficiency differences between the thin absorbers and the segmented approach and SaS calculated the angular dependence and the energy yield. Grid design was conceived by CVB and simulated and optimised by ShS. PS and PA did the fabrication process and electrical characterisation, and MM did the window and grid deposition. AD and RP characterised the AVT and the different device areas. All authors helped revise the manuscript.

Conflicts of interest

There are now conflicts to declare.

Data availability

Data is available upon request from the corresponding authors.

Supplementary information (SI) is available. See DOI: https://doi.org/10.1039/d5el00187k.

Acknowledgements

The authors acknowledge support by the project "Semi-TranspARent SOLar cells for building integrated photovoltaics (STAR-SOL)", funded by FCT - Fundação para a Ciência e a Tecnologia (FCT-FNR/0001/2018) and the Fond National de la Recherche (C18/MS/12686759). The research was partially funded by the European Union under the project "Hi-BITS – High efficiency bifacial thin film chalcogenide solar cells" (Grant Agreement no. 101122203). Views and opinions expressed are however those of the author(s) only and do not necessarily reflect those of the European Union. Neither the European Union nor the granting authority can be held responsible for them. The authors would like to sincerely thank the reviewers for their critical assessment and helpful comments, which greatly assisted to improve the manuscript.

References

1 D. Bogdanov, M. Ram, A. Aghahosseini, A. Gulagi, A. S. Oyewo, M. Child, U. Caldera, K. Sadovskaia, J. Farfan, L. De Souza Noel Simas Barbosa, M. Fasihi, S. Khalili, T. Traber and C. Breyer, Low-Cost Renewable Electricity as the Key Driver of the Global Energy Transition towards Sustainability, *Energy*, 2021, **227**, 120467, DOI: 10.1016/j.energy.2021.120467.

2 M. Z. Jacobson, A.-K. von Krauland, S. J. Coughlin, E. Dukas, A. J. H. Nelson, F. C. Palmer and K. R. Rasmussen, Low-Cost Solutions to Global Warming, Air Pollution, and Energy Insecurity for 145 Countries, *Energy Environ. Sci.*, 2022, **15**(8), 3343–3359, DOI: 10.1039/D2EE00722C.

3 H. S. Boudet, Public Perceptions of and Responses to New Energy Technologies, *Nat. Energy*, 2019, **4**(6), 446–455, DOI: 10.1038/s41560-019-0399-x.

4 European Commission. In focus: Energy efficiency in buildings. Energy efficiency in buildings. https://commission.europa.eu/news/focus-energy-efficiency-buildings-2020-02-17_en (accessed 2023-12-11).

5 E. P. Thompson, E. L. Bombelli, S. Shubham, H. Watson, A. Everard, V. D'Ardes, A. Schievano, S. Bocchi, N. Zand, C. J. Howe and P. Bombelli, Tinted Semi-Transparent Solar Panels Allow Concurrent Production of Crops and Electricity on the Same Cropland, *Adv. Energy Mater.*, 2020, **10**(35), 2001189, DOI: 10.1002/aenm.202001189.

6 C. Yang, D. Liu, M. Bates, M. C. Barr and R. R. Lunt, How to Accurately Report Transparent Solar Cells, *Joule*, 2019, **3**(8), 1803–1809, DOI: 10.1016/j.joule.2019.06.005.

7 S. Lehrl, K. Gerstmeyer, J. H. Jacob, H. Frieling, A. W. Henkel, R. Meyrer, J. Wiltfang, J. Kornhuber and S. Bleich, Blue Light Improves Cognitive Performance, *J. Neural Transm.*, 2007, **114**(4), 457–460, DOI: 10.1007/s00702-006-0621-4.

8 C. J. Traverse, R. Pandey, M. C. Barr and R. R. Lunt, Emergence of Highly Transparent Photovoltaics for Distributed Applications, *Nat. Energy*, 2017, **2**(11), 849–860, DOI: 10.1038/s41560-017-0016-9.

9 K. Lee, H.-D. Um, D. Choi, J. Park, N. Kim, H. Kim and K. Seo, The Development of Transparent Photovoltaics, *Cell Rep. Phys. Sci.*, 2020, **1**(8), 100143, DOI: 10.1016/j.xcrp.2020.100143.

10 C. Peng, Y. Huang and Z. Wu, Building-Integrated Photovoltaics (BIPV) in Architectural Design in China, *Energy Build.*, 2011, **43**(12), 3592–3598, DOI: 10.1016/j.enbuild.2011.09.032.

11 K. Nakayama, S. Shimojo and G. H. Silverman, Stereoscopic Depth: Its Relation to Image Segmentation, Grouping, and the Recognition of Occluded Objects, *Perception*, 1989, **18**(1), 55–68, DOI: 10.1068/p180055.

12 K. Lee, N. Kim, K. Kim, H.-D. Um, W. Jin, D. Choi, J. Park, K. J. Park, S. Lee and K. Seo, Neutral-Colored Transparent Crystalline Silicon Photovoltaics, *Joule*, 2020, **4**(1), 235–246, DOI: 10.1016/j.joule.2019.11.008.

13 M. Paire, C. Jean, L. Lombez, S. Collin, J.-L. Pelouard, I. Gérard, J.-F. Guillemoles and D. Lincot, Cu(In,Ga)Se2 Mesa Diodes for the Study of Edge Recombination, *Thin Solid Films*, 2015, **582**, 258–262, DOI: 10.1016/j.tsf.2014.11.033.

14 R. Scheer and H.-W. Schock, *Chalcogenide Photovoltaics: Physics, Technologies, and Thin Film Devices*, Wiley-VCH Verlag GmbH & Co. KGaA, 2011, DOI: 10.1002/9783527633708.

15 S. Siebentritt, E. Avancini, M. Bär, J. Bombsch, E. Bourgeois, S. Buecheler, R. Carron, C. Castro, S. Duguay, R. Félix, E. Handick, D. Hariskos, V. Havu, P. Jackson, H.-P. Komsa, T. Kunze, M. Malitckaya, R. Menozzi, M. Nesladek, N. Nicoara, M. Puska, M. Raghuwanshi, P. Pareige, S. Sadewasser, G. Sozzi, A. N. Tiwari, S. Ueda, A. Vilalta-Clemente, T. P. Weiss, F. Werner, R. G. Wilks, W. Witte and M. H. Wolter, Heavy Alkali Treatment of Cu(In,Ga)Se2 Solar Cells: Surface versus Bulk Effects, *Adv. Energy Mater.*, 2020, **10**(8), 1903752, DOI: 10.1002/aenm.201903752.

16 T. Sidali, A. Bou, D. Coutancier, E. Chassaing, B. Theys, D. Barakel, R. Garuz, P.-Y. Thoulon and D. Lincot, Semi-Transparent Photovoltaic Glazing Based on Electrodeposited CIGS Solar Cells on Patterned Molybdenum/Glass Substrates, *EPJ Photovoltaics*, 2018, **9**, 2, DOI: 10.1051/epjpv/2017009.

17 A. Jeong, J. M. Choi, H.-J. Lee, G. Y. Kim, J.-K. Park, W. M. Kim, S. Kuk, Z. Wang, D. J. Hwang, H. Yu and J. Jeong, Transparent Back-Junction Control in Cu(In,Ga)Se2 Absorber for High-Efficiency, Color-Neutral, and Semitransparent Solar Module, *Prog. Photovoltaics Res. Appl.*, 2022, **30**(7), 713–725, DOI: 10.1002/pip.3520.

18 D. B. Ritzer, B. A. Nejand, M. A. Ruiz-Preciado, S. Gharibzadeh, H. Hu, A. Diercks, T. Feeney, B. S. Richards, T. Abzieher and U. W. Paetzold, Translucent Perovskite Photovoltaics for Building Integration, *Energy Environ. Sci.*, 2023, **16**(5), 2212–2225, DOI: 10.1039/D2EE04137E.

19 P. M. P. Salomé, B. Vermang, R. Ribeiro-Andrade, J. P. Teixeira, J. M. V. Cunha, M. J. Mendes, S. Haque,

J. Borme, H. Águas, E. Fortunato, R. Martins, J. C. González, J. P. Leitão, P. A. Fernandes, M. Edoff and S. Sadewasser, Passivation of Interfaces in Thin Film Solar Cells: Understanding the Effects of a Nanostructured Rear Point Contact Layer, *Adv. Mater. Interfaces*, 2018, **5**(2), 1701101, DOI: 10.1002/admi.201701101.

20 M. Doroshenko, S. Keshav and C. Rosenberg, Flattening the Duck Curve Using Grid-Friendly Solar Panel Orientation, in *Proceedings of the Ninth International Conference on Future Energy Systems; E-Energy '18*, Association for Computing Machinery, New York, NY, USA, 2018, pp 375–377, DOI: 10.1145/3208903.3212029.

21 J. Lindahl, U. Zimmermann, P. Szaniawski, T. Törndahl, A. Hultqvist, P. Salomé, C. Platzer-Björkman and M. Edoff, Inline Cu(In,Ga)Se_2 Co-Evaporation for High-Efficiency Solar Cells and Modules, *IEEE J. Photovoltaics*, 2013, **3**(3), 1100–1105, DOI: 10.1109/JPHOTOV.2013.2256232.

22 A. R. Burgers, How to Design Optimal Metallization Patterns for Solar Cells, *Prog. Photovoltaics Res. Appl.*, 1999, **7**(6), 457–461, DOI: 10.1002/(SICI)1099-159X(199911/12)7:6%253C457::AID-PIP278%253E3.0.CO;2-U.

23 P. Santos, P. Anacleto, D. Brito, S. Shital, R. G. Poeira, A. Debot, P. J. Dale and S. Sadewasser, Fabrication of Semi-Transparent Cu(In,Ga)Se2 Solar Cells Aided by Bromine Etching, *Thin Solid Films*, 2023, **770**, 139778, DOI: 10.1016/j.tsf.2023.139778.

24 M. J. Shin, A. Lee, J. H. Park, A. Cho, S. K. Ahn, D. Shin, J. Gwak, J. H. Yun, J. Yoo and J.-S. Cho, Ultrathin Cu(In,Ga)Se2 Transparent Photovoltaics: An Alternative to Conventional Solar Energy-Harvesting Windows, *Nano Energy*, 2022, **92**, 106711, DOI: 10.1016/j.nanoen.2021.106711.

25 J. Park, K. Lee, J. Lee, D. Kim, M. Lee and K. Seo, All-Back-Contact Neutral-Colored Transparent Crystalline Silicon Solar Cells Enabling Seamless Modularization, *Proc. Natl. Acad. Sci. U. S. A.*, 2024, **121**(33), e2404684121, DOI: 10.1073/pnas.2404684121.

26 P. Jackson, D. Hariskos, R. Wuerz, O. Kiowski, A. Bauer, T. M. Friedlmeier and M. Powalla, Properties of Cu(In,Ga) Se2 Solar Cells with New Record Efficiencies up to 21.7%, *Phys. Status Solidi RRL*, 2015, **9**(1), 28–31, DOI: 10.1002/pssr.201409520.

27 Photovoltaic Geographical Information System (PVGIS) - European Commission. https://joint-research-centre.ec.europa.eu/photovoltaic-geographical-information-system-pvgis_en (accessed 2024-01-18).

28 N. Arora, SPICE Diode and MOSFET Models and Their Parameters, in *MOSFET Models for VLSI Circuit Simulation: Theory and Practice*, ed. N. Arora, Computational Microelectronics, Springer, Vienna, 1993, pp. 536–562, DOI: 10.1007/978-3-7091-9247-4_11.

29 G. T. Koishiyev and J. R. Sites, Impact of Sheet Resistance on 2-D Modeling of Thin-Film Solar Cells, *Sol. Energy Mater. Sol. Cells*, 2009, **93**(3), 350–354, DOI: 10.1016/j.solmat.2008.11.015.

30 LTspice Information Center | Analog Devices, https://www.analog.com/en/design-center/design-tools-and-calculators/ltspice-simulator.html, (accessed 2024-01-18).

31 N. Brum, PyLTSpice: A Set of Tools to Automate LTSpice Simulations, https://github.com/nunobrum/PyLTSpice, (accessed 2024-01-18).

32 PyGAD - Python Genetic Algorithm! — PyGAD 3.2.0 documentation, https://pygad.readthedocs.io/en/latest/, (accessed 2024-01-18).